2014 IEEE International Conference on Robotics & Automation (ICRA)
Hong Kong Convention and Exhibition Center
May 31 - June 7, 2014. Hong Kong, China

Instantaneous Ego-Motion Estimation using Multiple Doppler Radars

Dominik Kellner[1], Michael Barjenbruch[1], Jens Klappstein[2], Jürgen Dickmann[2] and Klaus Dietmayer[1]

Abstract— **The estimation of the ego-vehicle's motion is a key capability for advanced driving assistant systems and mobile robot localization. The following paper presents a robust algorithm using radar sensors to instantly determine the complete 2D motion state of the ego-vehicle (longitudinal, lateral velocity and yaw rate). It evaluates the relative motion between at least two Doppler radar sensors and their received stationary reflections (targets). Based on the distribution of their radial velocities across the azimuth angle, non-stationary targets and clutter are excluded. The ego-motion and its corresponding covariance matrix are estimated. The algorithm does not require any preprocessing steps such as clustering or clutter suppression and does not contain any model assumptions. The sensors can be mounted at any position on the vehicle. A common field of view is not required, avoiding target association in space. As an additional benefit, all targets are instantly labeled as stationary or non-stationary.**

I. Introduction

Standard vehicle odometry is performed by a combination of wheel-based odometry and inertial sensing (gyroscopes and accelerometers). Inertial sensors are prone to drift, which is compensated with periodic GPS absolute position updates. On high-traction terrain and with good GPS reception these systems provide an accurate motion estimation. But especially in slippery terrain or during high-dynamic maneuvers wheel speed sensors contain non-systematic errors due to wheel slip and slide. They have systematic errors caused by kinematic imperfections, unequal wheel diameters or uncertainties about the exact wheelbase.

The growing use of Doppler radars in the automotive field and continuously increasing measurement accuracy are opening new possibilities for a fast and reliable ego-motion estimation. It is based on the motion of the ego-vehicle relative to stationary radar targets. It is insensitive to the interaction of the vehicle to the ground and estimates the full 2D motion state. The motion estimation is free of bias and drift. This approach is becoming more feasible as the importance and number of radar systems in future automotive safety systems is growing.

This paper is organized as follows: Section II reviews related work. Section III gives an overview of the system and describes in detail the three main steps of the algorithm. Simulation results and the influence of crucial system parameters are discussed in Section IV. Section V contains the experimental results.

[1]Dominik Kellner, Michael Barjenbruch and Klaus Dietmayer are with driveU / Institute of Measurement, Control and Microtechnology Ulm, Germany dominik.kellner@uni-ulm.de

[2]Jens Klappstein and Jürgen Dickmann are with Daimler AG Ulm, Germany

II. Related Work

In this section only approaches, which are able to estimate the full 2D ego-motion with 3 degrees of freedom (DOF), are presented. The two major methods are visual odometry and wheel-based odometry, combined with GPS or an Inertial Measurement Unit (IMU). The main application areas are robot localization in rough terrain (e.g. [1]–[4]) and advanced driver assistant systems (e.g. [5]–[7]).

A. Visual Odometry

Visual odometry estimates the vehicle motion from a sequence of camera images and can be categorized as being either monocular or stereoscopic, and employing either feature tracking or feature matching [3]. Using stereo vision, the 3D points can be reconstructed using triangulation, and point features are found using e.g. the iterated closest point approach. Monocular cameras primarily require tracking image features over a certain number of images. The scene can be reconstructed using structure from motion. In most cases stereo outperforms monocular visual odometry [5].

To avoid tracking image features over multiple frames the feature correspondence between two consecutive frames can be used [6]. The ego-motion of a vehicle is estimated using the trifocal tensor which relates features between three images of the same static scene. Simulation results show a position error of circa 30 m (1.5%) for a travel distance of 2000 m, and a standard deviation of approximately 15 m (0.8%).

In [5], stereo is computed for every frame obtaining 3D points. Using the optical flow, point correspondence is established in two consecutive frames. The ego-motion of a vehicle is estimated using a closed form solution based on quaternions. The error for a loop-close after circa 700 m is 17 m (2.4%).

A combination of stereo vision with robust frame-to-frame motion estimation, an inexpensive inertial measurement unit (if visual odometry fails) and a low-cost GPS sensor (to prevent long-term drift) is presented in [8]. The achieved position error for four loop closing scenes in an outdoor environment is 2.2%-5.0% with solely visual odometry and 0.3%-2.0% for the combination with GPS.

B. Wheel-based odometry and inertial measurements

Estimating the full motion state with current vehicle's odometry is still a critical task, since the vehicle's side-slip can be measured directly only by speed over ground sensors or multiple antenna GPS attitude systems. A good overview of current approaches is presented in [9]. The common approach is the determination by the integration of

978-1-4799-3684-7/14/$31.00 ©2014 IEEE

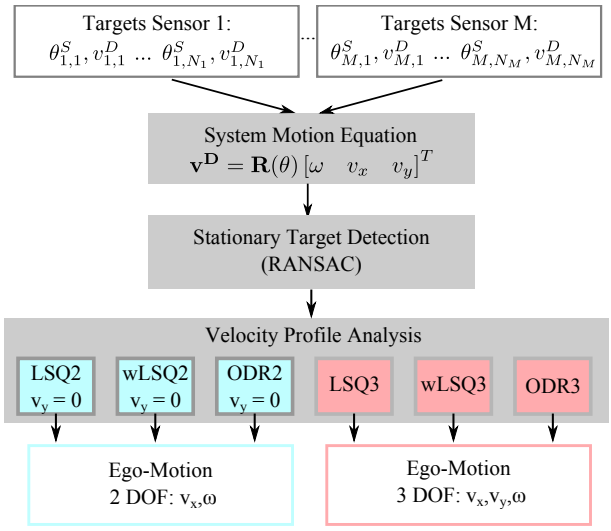

Fig. 1. Overview of the different system steps

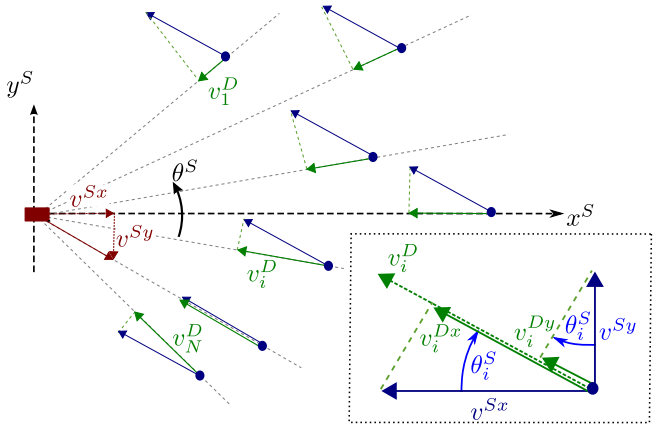

Fig. 2. From all stationary targets the radial part (green arrow) of the relative velocity (blue arrow) is measured by the Doppler radar

inertial sensors and steer angle measurements. Side-slip can be estimated only through the extension of velocity heading information.

There are a variety of systems presented using Kalman filters with extended sensors to enhance wheel-based odometry. A combination of classic odometry and inertial measurements is used in [2]. In [7] inertial sensors, odometry and D-GPS are used to estimate the slip for a vehicle at high speed. In [4] a combination of visual odometry, IMU and wheel rates is used for a Mars rover. The approach of [10] is only based on a low cost IMU.

C. Radar-based ego-motion

No existing radar-based system, which is able to estimate the full motion state of a vehicle based on a single measurement cycle is known to the authors. For an overview of relative and absolute position measurement using radar sensors the reader is referred to [11]. The presented systems are based on a single radar and can only determine the velocity vector of the radar (2 DOF), but not full 2D vehicle motion state (3 DOF).

Compared to visual odometry, radar-based systems have the advantage that Doppler radar sensors can directly measure the relative velocity of stationary objects in a single measurement, avoiding the derivation by the changing position over two or more consecutive frames. Compared to IMU, the estimation of motion parameters is not influenced by drift or scaling factors.

III. EGO-MOTION ESTIMATION ALGORITHM

Fig. 1 provides an overview of the ego-motion estimation system. An arbitrary number of Doppler radar sensors with known position and orientation are mounted on the vehicle, measuring at each time step an arbitrary number of targets. The azimuth position and radial velocity of each target is registered and evaluated using the *System Motion Equation*. Subsequently stationary targets are identified by a statistical evaluation of this equation. In the final step different algorithms can be used to solve the ego-motion state problem and its corresponding covariance matrix. For a 2 DOF estimation at least two targets and for a 3 DOF estimation three targets (from at least two sensors) have to be captured.

A. Sensor Measurement Equation

If a radar sensor $j \in \{1, ..., M\}$ is moved, from its point of view all stationary targets move in the opposite direction (Fig. 2). The relative velocity of a stationary target $i_j \in \{1, ..., N_j\}$ is equal to the inverse sensor velocity vector (v_j^{Sx},v_j^{Sy}). The radar measures only the corresponding radial (Doppler-) velocities of this vector ($v^D_{j,i}$), depending on the azimuth position ($\theta^S_{j,i}$). Combining all stationary targets from one sensor results in:

$$\begin{bmatrix} -v^D_{j,1} \\ \vdots \\ -v^D_{j,N_j} \end{bmatrix} = \begin{bmatrix} \cos(\theta^S_{j,1}) & \sin(\theta^S_{j,1}) \\ \vdots & \vdots \\ \cos(\theta^S_{j,N_j}) & \sin(\theta^S_{j,N_j}) \end{bmatrix} \begin{bmatrix} v_j^{Sx} \\ v_j^{Sy} \end{bmatrix} \quad (1)$$

The azimuth position is in the local sensor coordinate system, as is the resulting velocity vector (v_j^{Sx},v_j^{Sy}). For the fusion of the velocity information of multiple sensors the velocity has to be transformed into a global coordinate system (v_j^x,v_j^y), depending on the sensor mounting orientation β_j:

$$\begin{bmatrix} v_j^{Sx} \\ v_j^{Sy} \end{bmatrix} = \begin{bmatrix} \cos(\beta_j) & \sin(\beta_j) \\ -\sin(\beta_j) & \cos(\beta_j) \end{bmatrix} \begin{bmatrix} v_j^x \\ v_j^y \end{bmatrix} \quad (2)$$

To avoid systematic errors a precise determination of the mounting orientation is required. Combining (1) and (2) with the global azimuth position $\theta_{j,i} = \beta_j + \theta^S_{j,i}$ leads to the global measurement equation:

$$\begin{bmatrix} -v^D_{j,1} \\ \vdots \\ -v^D_{j,N_j} \end{bmatrix} = \underbrace{\begin{bmatrix} \cos(\theta_{j,1}) & \sin(\theta_{j,1}) \\ \vdots & \vdots \\ \cos(\theta_{j,N_j}) & \sin(\theta_{j,N_j}) \end{bmatrix}}_{\mathbf{M_j}} \begin{bmatrix} v_j^x \\ v_j^y \end{bmatrix} \quad (3)$$

$$\mathbf{v_j^D} = \mathbf{M_j}\,\mathbf{v_j}$$

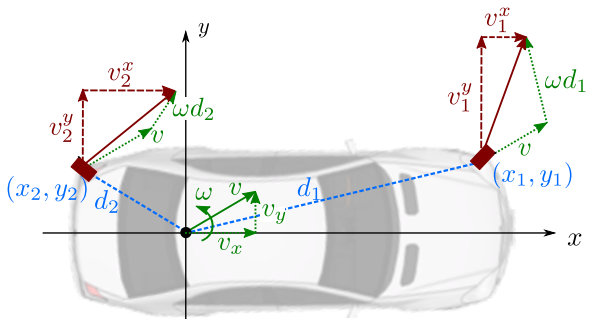

Fig. 3. Vehicle motion specified at reference point (middle of rear axis) and the corresponding sensor motion (red - v_j^x,v_j^y) at position (blue - x_j,y_j)

B. System Motion Equation

The motion of an arbitrary rigid object is fully described by the reference point velocity (v_x,v_y) and yaw rate ω of the object. The reference point is arbitrary and set to the middle of the rear axis, with the x-axis parallel and the y-axis orthogonal to the moving direction as outlined in Fig. 3. The sensor positions are described in system coordinates as (x_j,y_j). The velocity vectors (v_j^x, v_j^y) of all sensors (j = 1 ... M) are given by the following equation system:

$$\begin{bmatrix} v_1^x \\ v_1^y \\ \vdots \\ v_M^x \\ v_M^y \end{bmatrix} = \underbrace{\begin{bmatrix} -x_1 & 1 & 0 \\ y_1 & 0 & 1 \\ \vdots & \vdots & \vdots \\ -x_M & 1 & 0 \\ y_M & 0 & 1 \end{bmatrix}}_{[\mathbf{v_1} \dots \mathbf{v_M}]^T \;=\; [\mathbf{S_1} \dots \mathbf{S_M}]^\mathbf{T}} \begin{bmatrix} \omega \\ v_x \\ v_y \end{bmatrix} \qquad \mathbf{s} \tag{4}$$

With the chosen reference point the Ackerman condition (no side-slip at the rear axis) can be introduced by deleting the last element of $\mathbf{s}$ and last column of $\mathbf{S}$. Eq. (3) can be rewritten for all sensors:

$$\begin{bmatrix} \mathbf{v_1^D} \\ \mathbf{v_2^D} \\ \vdots \\ \mathbf{v_M^D} \end{bmatrix} = \begin{bmatrix} \mathbf{M_1} & \mathbf{0} & \dots & \mathbf{0} \\ \mathbf{0} & \mathbf{M_2} & \dots & \mathbf{0} \\ \vdots & \vdots & \ddots & \vdots \\ \mathbf{0} & \mathbf{0} & \dots & \mathbf{M_M} \end{bmatrix} \begin{bmatrix} \mathbf{v_1} \\ \mathbf{v_2} \\ \vdots \\ \mathbf{v_M} \end{bmatrix} \tag{5}$$

The complete system motion equation is a combination of (4) and (5):

$$\begin{bmatrix} \mathbf{v_1^D} \\ \mathbf{v_2^D} \\ \vdots \\ \mathbf{v_M^D} \end{bmatrix} = \begin{bmatrix} \mathbf{M_1 S_1} \\ \mathbf{M_2 S_2} \\ \vdots \\ \mathbf{M_j S_j} \end{bmatrix} \begin{bmatrix} \omega \\ v_x \\ v_y \end{bmatrix} \tag{6}$$

$$\mathbf{v^D} \quad = \quad \mathbf{R} \qquad \mathbf{s}$$

C. Stationary Target Detection

A RANdom SAmple Consensus (RANSAC) algorithm is used to identify the major group of targets with the same velocity profile, assuming they all belong to stationary objects. In each iteration, three targets from at least two different sensors are randomly chosen and the parameters of their velocity profile ($\mathbf{s}$) are determined using (6). The

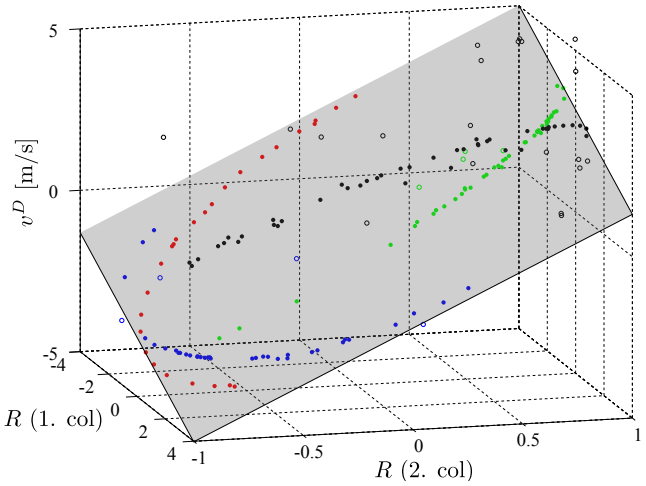

Fig. 4. The estimated velocity parameters are represented as a plane (gray) in the $\mathbf{R}$-$\mathbf{v^D}$ space. All targets from the two sensors in the front (red, blue) and in the back (green, black) are shown in this space. They can be divided into inliers (filled) and outlier (empty).

error of the current fit is calculated by the sum of the radial velocity errors of all targets to the determined velocity profile of the current fit. In this process a corridor threshold is used to identify outliers and limit their error to the corridor threshold. After a certain number of iterations (result-driven), the best fit is chosen, according to the calculated error and/or number of inliers. All outliers are considered as either moving objects or clutter and excluded. All inliers are used in the velocity profile analysis introduced in the next section. Fig. 4. shows an example for the 2 DOF case, in which the solution $\mathbf{s}$ is a plane in the 3D space. The algorithm only fails if there is another group of objects, which all have exactly the same linear movement and their number of received targets is larger than of the stationary objects in all sensors. Possible solutions in this case are presented in [11].

D. Velocity Profile Analysis

A Least-SQuares estimator (LSQ) is optimal if measurement errors are only present in the dependent variable v^D. An azimuth position error θ in $\mathbf{M}$ is interpreted as radial velocity error, as shown in Fig. 5. Depending on the position in the velocity profile the accuracy of each target varies significantly. With an increasing shift of the velocity profile, the impact of an azimuth position error increases.

A simple solution to compensate for the azimuth position error is a weighting factor dependent on its position in the velocity profile (wLSQ). It can be calculated, e.g., by determining the amplitude roughly by an unweighted LSQ estimator and then calculating the weights according to the ratio of its radial velocity to the velocity profile's amplitude. Simulation results show an increasing accuracy especially for a larger azimuth measurement error σ_θ and a faster object motion, causing larger deviations in the velocity profile.

An optimal solution is obtained using an Orthogonal Distance Regression (ODR), which considers not only a radial velocity, but also an azimuth measurement error. It minimizes the error of all targets with respect to their measurement

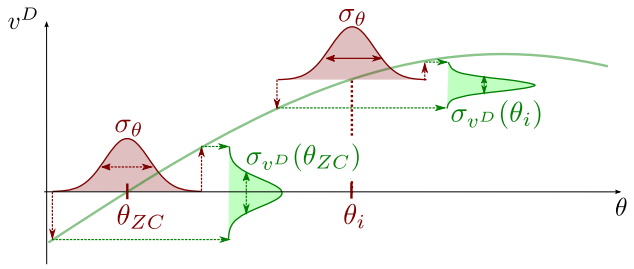

Fig. 5. Influence of a constant azimuth measurement error (σ_θ - green) on the radial velocity error (σ_{v^D} - red) depending on the target azimuth position (θ) using an ordinary LSQ-estimator. The maximal σ_{v^D} is at the zero-crossing θ_{ZC} (largest gradient) of the velocity profile.

covariances σ_θ and σ_{v^D}. This approach is described in [12] in detail. The optimization problem is solved by a two-stage Levenberg-Marquardt algorithm with the LSQ solution as initial guess. The superior algorithm searches the best system candidate $\hat{\mathbf{s}}$, using the orthogonal error obtained by the subordinated algorithm and a numerical determination of the Jacobian matrix. The subordinated algorithm estimates the velocity profile parameters $\mathbf{v_j}$ based on the current system candidate $\hat{\mathbf{s}}$ using (4) and then the total orthogonal error of all targets independently for each sensor.

The accuracy of the estimated motion parameters are influenced by a number of system parameters as discussed in Section IV. Depending on the subsequent processing step (e.g. Kalman filter) an estimate of the covariance matrix for the ascertained parameters is desirable. The covariance of a linear equation system (6) can be calculated using its inverse Hessian matrix [13]. In this case the covariance matrix is computed based on the variance of all targets and the number of DOF n_{DOF}:

$$Cov(\mathbf{s}) = \frac{(\epsilon^T \epsilon)(\mathbf{R^T R})^{-1}}{(\sum_{j=1}^{M} N_j) - n_{\mathrm{DOF}}} \tag{7}$$

$$\text{with: } \epsilon = \mathbf{R}\,\mathbf{s} - \mathbf{v^D}$$

IV. Simulation Results

A. Simulation Overview

The performance of the algorithm is investigated by simulating a vehicle with four sensors at each corner (field of view +/- 40°). The measurement uncertainties of the radar sensors (f_{cycle} = 20 Hz) are σ_θ = 1° and σ_{v^D} = 0.1 m/s. Both errors are supposed to be zero-mean Gaussian distributions. It is assumed that 100 stationary reflections are randomly distributed in the field of views of all radar sensors. The simulated route consists of four straight parts (v = 10 m/s, t = 6 s) and four constant turn parts (v = 10 m/s, ω = 15°/s, t = 6 s), resulting in a loop with a total distance of 480 m. In a variation, a small side-slip (v_y = 0.1 m/s) is added during turns. A Monte-Carlo simulation with 10 000 trials was carried out.

B. Algorithm Comparison

After a complete round-trip the absolute position (d) and motion parameter (ω,v) errors are examined for the proposed algorithms in Table I.

TABLE I

Simulation Results: v_y = 0.0m/s (top) and v_y = 0.1m/s (bottom) in terms of standard deviation (bias error)

v_y = 0 m/s	d [m]	$\omega[°/s]$	v [m/s]
LSQ2	1.97 (1.59)	6.9e-1 (2.6e-2)	1.9e-2 (1.6e-3)
wLSQ2	1.95 (1.60)	6.9e-1 (3.9e-2)	**1.8e-2 (8.0e-4)**
ODR2	**1.88 (0.07)**	**6.7e-1 (2.0e-4)**	**1.7e-2 (1.1e-3)**
LSQ3	2.24 (0.40)	8.0e-1 (5.6e-3)	1.9e-2 (2.1e-3)
wLSQ3	2.24 (0.54)	8.1e-1 (8.5e-3)	**1.8e-2 (9.0e-4)**
ODR3	2.12 (0.21)	7.8e-1 (2.1e-3)	**1.7e-2 (1.1e-3)**

v_y = 0.1 m/s	d [m]	$\omega[°/s]$	v [m/s]
LSQ2	2.26 (40.7)	9.4e-1 (6.0e-1)	2.2e-2 (1.3e-2)
wLSQ2	2.18 (46.1)	1.0e-0 (6.8e-1)	2.0e-2 (7.9e-3)
ODR2	2.16 (47.7)	9.7e-1 (7.0e-1)	1.9e-2 (6.3e-3)
LSQ3	2.40 (0.19)	8.0e-1 (2.1e-3)	1.9e-2 (1.9e-3)
wLSQ3	2.32 (0.28)	8.1e-1 (3.5e-3)	**1.8e-2 (7.0e-4)**
ODR3	**2.29 (0.10)**	**7.8e-1 (1.5e-3)**	**1.8e-2 (1.3e-3)**

The key findings of the simulations are:

1) The system shows a promising accuracy with a standard deviation in end position $<$ 2.5 m (0.6%) and end orientation ($<$ 0.8°) and a bias free 3 DOF estimation.
2) A small side-slip causes a significant position ($>$ 40 m) and yaw-rate bias ($>$ 0.6°) in the 2 DOF estimators, whereas the velocity error is stable.
3) A side-slip has no influence on the 3 DOF estimators.
4) The velocity estimation and end position is more accurate for wLSQ than LSQ.
5) ODR is bias free and most accurate for all parameters, but is subject to a longer execution time.

C. Influence of system parameters

The quality of the results depends strongly on a large number of parameters, and is analyzed for the yaw-rate estimation of ODR2 and ODR3 in this section:

1) Motion parameters (velocity, yaw rate and their fluctuations)
2) Environmental parameters (number of stationary targets at each sensor, non-stationary targets and clutter and the distribution of the targets inside the fields of view)
3) Sensor parameters (number of sensors, mounting position and orientation, azimuth and velocity measurement accuracy, field of view and sampling rate)

The first simulation examines the influence of the motion parameters (Fig. 6). With increasing velocity the error increases roughly linearly. With increasing drift ($v_y > 0$) the ODR2 bias error increases linearly and for v_y = 0.09 m/s it is larger than the standard deviation of the ODR3. The standard deviation of ODR2 is less than that of ODR3 only for a drift less than v_y = 0.06 m/s. There is no influence of the drift on the accuracy of ODR3. The yaw-rate of the vehicle has a negligible influence on the results (not shown).

The second simulation examines the effect of the environmental parameters (Fig. 7). The standard deviations decrease roughly with the inverse square root of the number of targets. To examine the effects of moving targets or clutter on the estimated parameters, targets with a random azimuth angle are added. They have a random radial velocity inside the range of the radial velocities of stationary objects. Increasing

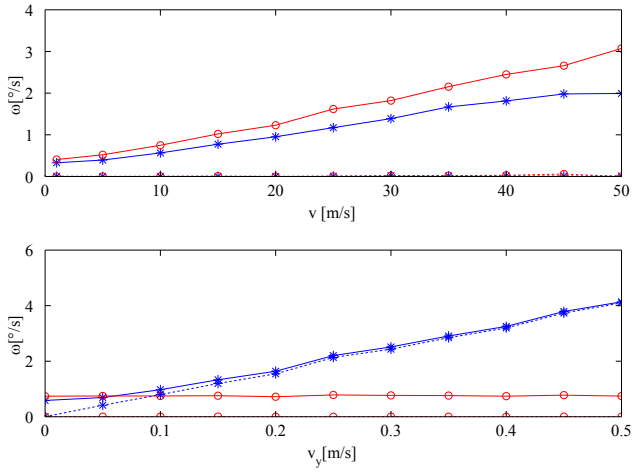

Fig. 6. Estimated yaw rate for ODR2 (*) and ODR3 (o) dependent on vehicle's velocity (v_y = 0) (top) and drift (bottom) in terms of standard deviation (solid) and bias error (dotted)

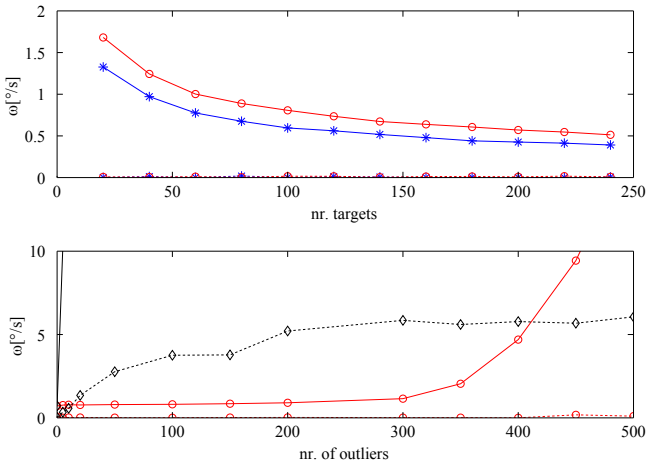

Fig. 7. Estimated yaw rate for ODR2 (*) and ODR3 (o) dependent on the number of stationary targets (top) and number of non-stationary targets of ODR3 (o) and ODR3 without outlier detection (◇) (bottom) in terms of standard deviation (solid) and bias error (dotted)

this range, the effects are weakened. For an equal number of non-stationary and stationary targets the standard deviation increases only with 8%, to double the standard deviation 330 non-stationary targets (100 stationary) are needed.

With increasing measurement error in azimuth σ_θ as well as radial velocity σ_{v^D}, the parameter errors increase almost linearly (not shown). A radial velocity error of 0.2 m/s is equal to an azimuth position error of 1.5°. The number of sensors, field of view and orientation can be reduced to the following two velocity profile parameters: covered azimuth area and number of targets. If the total covered azimuth area is larger than 180°, increasing area has only a minor influence on the system's accuracy, since both amplitude and phase-shift of the velocity profile can be interpolated. For smaller azimuth areas the accuracy decreases slightly. The field of view has only a small influence for one or two sensors and a covered azimuth area smaller than 180°. The accuracy increases with a larger spatial distribution of the mounting positions of the sensors.

V. Experiments

A. Example Sequence

An example sequence with two high-resolution Doppler radars (σ_{v^D} = 0.1 m/s, $\sigma_\theta = 1°$) mounted on both sides in front of the vehicle is shown in Fig. 8. The results are visualized by integrating the estimated ego-motion over the complete sequence (60 s and approximately 300 m). Due to the integration over a large time range, minimal errors in the estimated yaw rate have a significant influence on the later position. At the first corner the surface was partly icy, resulting in an odometry error due to a side-slip. This error in odometry is integrated over time resulting in a large position error at the end of the route. However, the proposed system is able to detect the side-slip angle and compensate it, resulting in a low end-position error. The current positions provided by ODR3 are used to build a grid-map. Only targets labeled as stationary are registered in the map. Free space, the road contour, buildings and the contour of parked cars are visible.

B. ADMA Benchmark

The second scenario is a figure-eight driven quickly in a parking lot ($v \approx$ 5-10 m/s). Four Doppler radar sensors (σ_{v^D} = 0.1 m/s, σ_θ = 1°) are mounted at each corner of the vehicle and combined using the proposed ODR3 algorithm to estimate the velocities at the rear axis and yaw rate. The standard wheel-based odometry is taken as a benchmark. Both methods are compared in terms of motion and end-position errors to an Automotive Dynamic Motion Analyzer (ADMA), a high precision Inertial Measurement Unit (IMU) with DGPS support. The final position is shown in Fig. 9.

On average, approximately 200 reflections are detected in each time step. The position estimation of ODR3 is highly accurate for this highly dynamic maneuver, with an error smaller than 1.1 m after circa 140 m (0.75%). The yaw-rate accuracy is almost equal, since the integrated yaw rate sensor is roughly independent of the dynamic of the maneuver. The velocity error is significant larger for the vehicle odometry. As shown in Fig. 10, its velocity error is strongly correlated to the yaw rate. The fast turns ($> 30°/s$) causes a small side-slip angle and wheel-slippage, which makes wheel-based odometry inaccurate as discussed in Section II.

VI. Conclusion

The presented relative position measurement system is based on two or more Doppler radar sensors. Independent of their mounting position and orientation, this system is able to estimate the full 2D motion state of the vehicle in just one measurement cycle using only sensors of existing or future safety systems. No additional components have to be mounted on the vehicle. The dynamic covariance matrix provides a quality criterion for the estimated parameters. Using this criterion, the system is able to replace or enhance current odometry systems in vehicles. It has been shown that the results remain stable even with a large number of moving objects or clutter in the field of view and also show promising accuracy in high dynamic maneuvers.

REFERENCES

[1] L. Ojeda, G. Reina, and J. Borenstein, "Experimental results from flexnav: An expert rule-based dead-reckoning system for mars rovers," in *Aerospace Conference, 2004. Proceedings. 2004 IEEE*, vol. 2, pp. 816–825, IEEE, 2004.

[2] Y. Fuke and E. Krotkov, "Dead reckoning for a lunar rover on uneven terrain," in *Robotics and Automation, 1996. Proceedings., 1996 IEEE International Conference on*, vol. 1, pp. 411–416, IEEE, 1996.

[3] A. Howard, "Real-time stereo visual odometry for autonomous ground vehicles," in *Intelligent Robots and Systems, 2008. IROS 2008. IEEE/RSJ International Conference on*, pp. 3946–3952, IEEE, 2008.

[4] D. M. Helmick, Y. Cheng, D. S. Clouse, L. H. Matthies, and S. I. Roumeliotis, "Path following using visual odometry for a mars rover in high-slip environments," in *Aerospace Conference, 2004. Proceedings. 2004 IEEE*, vol. 2, pp. 772–789, IEEE, 2004.

[5] H. Badino, "A robust approach for ego-motion estimation using a mobile stereo platform," in *Complex Motion*, pp. 198–208, Springer, 2007.

[6] B. Kitt, A. Geiger, and H. Lategahn, "Visual odometry based on stereo image sequences with ransac-based outlier rejection scheme," in *Intelligent Vehicles Symposium (IV), 2010 IEEE*, pp. 486–492, IEEE, 2010.

[7] M. Wada, K. S. Yoon, and H. Hashimoto, "High accuracy road vehicle state estimation using extended kalman filter," in *Intelligent Transportation Systems, 2000. Proceedings. 2000 IEEE*, pp. 282–287, IEEE, 2000.

[8] M. Agrawal and K. Konolige, "Real-time localization in outdoor environments using stereo vision and inexpensive gps," in *Pattern Recognition, 2006. ICPR 2006. 18th International Conference on*, vol. 3, pp. 1063–1068, IEEE, 2006.

[9] R. Anderson and D. M. Bevly, "Estimation of slip angles using a model based estimator and gps," in *American Control Conference, 2004. Proceedings of the 2004*, vol. 3, pp. 2122–2127, IEEE, 2004.

[10] B. Barshan and H. F. Durrant-Whyte, "Inertial navigation systems for mobile robots," *Robotics and Automation, IEEE Transactions on*, vol. 11, no. 3, pp. 328–342, 1995.

[11] D. Kellner, M. Barjenbruch, J. Klappstein, J. Dickmann, and K. Dietmayer, "Instantaneous ego-motion estimation using doppler radar," in *Intelligent Transportation Systems (ITSC), 2013 16th International IEEE Conference on*, IEEE, 2013.

[12] D. Kellner, M. Barjenbruch, J. Klappstein, J. Dickmann, and K. Dietmayer, "Instantaneous lateral velocity estimation of a vehicle using doppler radar," in *Information Fusion (FUSION), 2013 16th International Conference on*, IEEE, 2013.

[13] C. D. Ghilani, *Adjustment computations: spatial data analysis*. John Wiley & Sons, 2010.

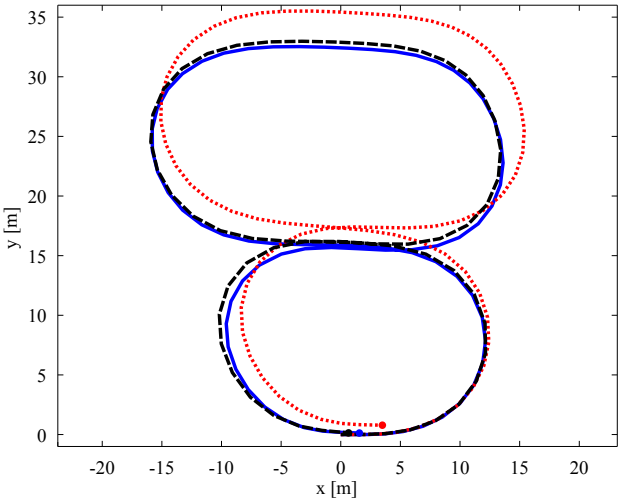

Fig. 9. Comparison of integrated radar ego-motion ODR3 (black-dashed), standard wheel-based odometry (red-dotted) and INS (black-solid) for a figure-eight driven in a parking lot (start at (0/0)). End points are marked.

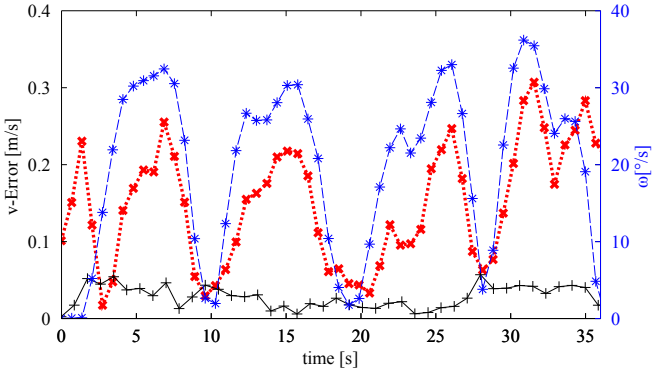

Fig. 10. Absolute velocity error of wheel-based odometry (red x) and radar ego-motion (black +), in relation to the absolute yaw rate of INS (blue *)

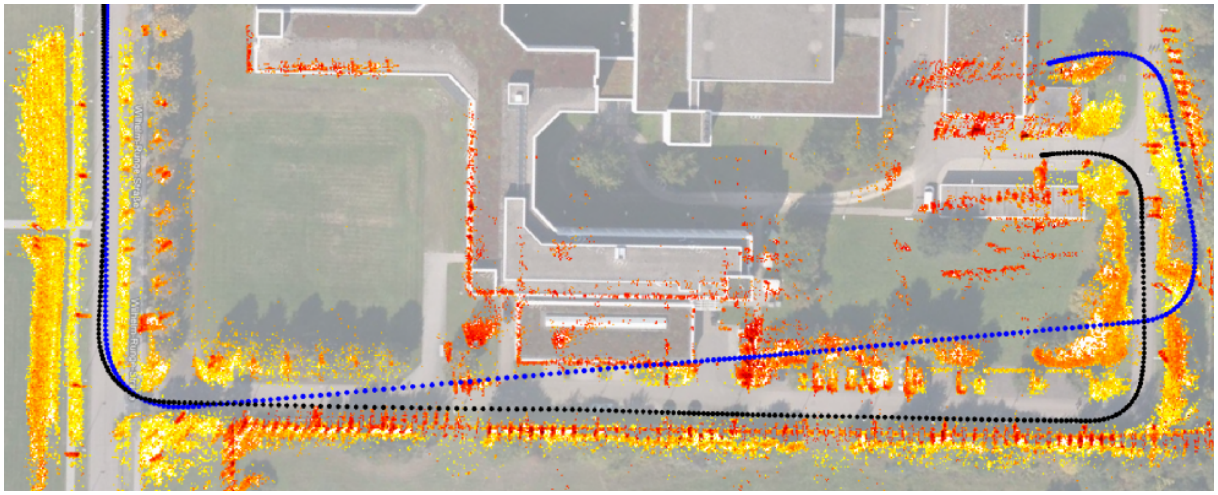

Fig. 8. Integrated ego-motion data of two radar sensors combined (black) and standard vehicle odometry (blue). Targets are mapped using radar-ego-motion and their intensity is represented by the color [yellow to red]. Start point: Top Left. (Aerial photography by GeoBasis-DE/BKG, Google)